IIETA International Information and Engineering Technology Association
Advancing the World of Information and Engineering

Mathematical Modelling of Engineering Problems
Vol. 12, No. 10, October, 2025, pp. 3667-3674
Journal homepage: http://iieta.org/journals/mmep

Assessing Rooftop Solar Potential for Photovoltaic Installations in Genoa: A GIS-Based Approach for Urban Energy Planning

Samuele Memme*, Marco Fossa, Davide Lepore, Stefano Morchio, Mattia Parenti, Antonella Priarone

DIME – Department of Mechanical, Energy, Management and Transportation Engineering, University of Genova, Genova 16145, Italy

Corresponding Author Email: samuele.memme@edu.unige.it

https://doi.org/10.18280/mmep.121030

Received: 10 September 2025
Revised: 14 October 2025
Accepted: 20 October 2025
Available online: 31 October 2025

Keywords:
GIS-based energy modelling, Renewable Energy Communities, rooftop PV, solar cadaster, urban solar energy potential

ABSTRACT

In response to the growing demand for decentralised renewable energy and the EU's push for carbon neutrality, the Italian region of Liguria, of which Genoa is the capital, faces the ambitious goal of increasing to 1,195 MW_p the installed photovoltaic capacity by 2030. In this context, Renewable Energy Communities (RECs) are emerging as a key mechanism to promote self-consumption and local energy production. This study proposes a GIS-based methodology for evaluating the rooftop solar potential of urban districts, using Genoa's Albaro neighbourhood as a case study. High-resolution LiDAR-based Digital Surface Models, vector building data, and Typical Meteorological Year (TMY) datasets were processed using the SEBE module within the UMEP plugin for QGIS. A cumulative sky model was implemented to account for local shading, surface tilt, and orientation. The analysis introduced a composite rooftop suitability index combining average annual insolation, usable surface area, and irradiance uniformity. Results show that around 34% of the rooftops meet the selected minimum criteria for PV deployment, with a theoretical potential of 45 MW_p comparable to the installed PV capacity of the entire province of Genoa. The study aims to highlight the value of solar cadastres as decision-support tools for RECs implementation, enabling prioritisation of high-performing surfaces in complex urban environments.

1. INTRODUCTION

Over the past decade, energy systems have undergone a notable transformation towards greater sustainability, marked by enhancements in efficiency and the decentralisation of renewable energy production. This evolution has catalysed a sharp rise in solar energy deployment, spurred by policy interventions from both national governments and international bodies seeking to address the escalating climate emergency. Additionally, the strategic imperative to diversify energy supply sources and mitigate reliance on external providers has reinforced the momentum of this transition. Within the European Union, photovoltaic (PV) technology has played a central role in this expansion, with the cumulative installed capacity reaching approximately 339.4 GW by the close of 2024, including an estimated 62.6 GW added in that year alone [1].

Over recent years, PV technology has evolved from a solution largely reserved for affluent single-family households into a widely accessible and economically viable option across diverse residential settings. In parallel, many European countries have progressively introduced regulatory frameworks that facilitate the development of PV sharing schemes and energy communities. Within this evolving landscape, digital solar platforms play an increasingly important role in promoting knowledge dissemination and fostering collaboration among stakeholders [2].

This type of sharing community has been formally recognised in Italy through the establishment of Renewable Energy Communities (RECs), i.e., legal entities composed of members such as citizens, small and medium enterprises, local authorities, associations, educational and research institutions, religious organisations, and environmental groups. These members collectively produce and share electricity from renewable sources for their own consumption, thus supporting a decentralised energy model by encouraging the deployment of small-scale renewable installations. The establishment of RECs was initiated with the implementation of the RED II Directive and was further formalized with the approval of the Configurazioni di autoconsumo per la condivisione dell'energia rinnovabile (CACER) and Testo Integrato per l'Autoconsumo Diffuso (TIAD) Decrees, by Autorità di Regolazione per Energia Reti e Ambiente (ARERA) and Italian Ministry of Environment and Energy Security (MASE).

Given that approximately 39% of the European population resides in urban centres and 36% in towns and suburbs [3], these densely populated areas present considerable opportunities for the integration of PV systems and the advancement of distributed energy generation. It is worth noting that, by 2024, over one-third of PV systems installed globally are located on rooftops [1], underscoring the relevance of urban buildings as key assets for solar energy

exploitation.

Within the framework of RECs, which are supported by dedicated regulatory and operational mechanisms, identifying suitable urban surfaces for solar deployment becomes a critical step. In this regard, solar assessment platforms, commonly referred to as solar cadasters, serve as key tools. These platforms integrate high-resolution spatial and meteorological data to provide accurate evaluations of solar potential across cityscapes, enabling stakeholders to identify rooftops that are viable for PV or solar thermal installations [4]. The effectiveness of such assessments relies heavily on accounting for critical factors such as surface tilt, azimuth, and shading from surrounding structures, which are known to influence annual insolation and energy yield across both thermal [5] and PV applications [6].

Although detailed city-scale solar platforms are still relatively scarce, increasing interest in assessing urban solar potential has led to a growing body of research aimed at developing solar cadasters and urban planning strategies. Among the notable initiatives are the regional solar cadastre of Geneva [7], as well as urban platforms in various French cities (e.g., Montpellier, Béziers, Nantes, Bordeaux) and German cities (e.g., Bremen, Hamburg, Kaiserslautern). Similar efforts have also been implemented in parts of Belgium, Luxembourg, the Netherlands, Norway, Poland, Spain, Sweden, and the United Kingdom. A comprehensive review and classification of these platforms, categorised into atlases, mapping, and cadasters, can be found in the study [8].

In this context, the present study introduces a methodology for estimating annual rooftop solar irradiation in a selected district of Genoa (44.4056°N, 8.9463°E), a Mediterranean city located in northern Italy. The approach employs Digital Surface Model (DSM) and LiDAR datasets, processed within a QGIS environment, to accurately account for the effects of slope and orientation of urban surfaces relevant for solar technology deployment. Beyond the evaluation of solar exposure, the study includes a series of statistical metrics to develop a composite interest index for PV potential, evaluated at a spatial resolution of 0.5 × 0.5 m². This index combines rooftop area, mean annual insolation, and intra-surface insolation variability to identify rooftops that receive uniform solar exposure throughout the year. This is essential, as spatial variability in sunlight, often caused by intermittent shading, can have a considerable impact on solar system performance.

2. THEORETICAL BACKGROUND

Solar irradiance reaching the Earth's surface comprises both direct and diffuse radiation components. When integrated over time, this quantity is referred to as insolation. Irradiance and insolation are generally measured on a horizontal plane, where the total incoming radiation is the sum of its direct and diffuse fractions. However, for surfaces inclined with respect to the horizontal, a correction factor known as R_b is introduced to account for the geometric effect of tilt on beam radiation availability. The instantaneous R_b factor represents the ratio between the direct beam irradiance on a tilted plane ($G_{b,T}$) and that on a horizontal plane ($G_{b,H}$), as in Eq. (1).

$$R_b = \frac{G_{b,T}}{G_{b,H}} = \frac{\cos(\theta_w)}{\cos(\theta)} \quad (1)$$

Mathematically, this is expressed as the ratio of the cosine of the incidence angle (θ_w) on the tilted surface to the cosine of the solar zenith angle (θ) on the horizontal plane.

An R_b value exceeding unity indicates that an inclined surface intercepts a greater fraction of direct solar radiation compared to a horizontal reference plane, whereas values below unity suggest a relative disadvantage in capturing beam radiation. For applications where time-averaged values are needed, e.g., for hourly or daily solar energy estimates, R_b can be calculated using integrated irradiance values, specifically H_h for hourly and H_d for daily data, instead of instantaneous measurements.

Accurately assessing the availability of solar resources on inclined surfaces is particularly crucial in urban contexts, where the geometry of the built environment introduces substantial complexity. In many cases, detailed measurements of sky radiance distributions are not available, making it necessary to rely on computational methods to estimate diffuse irradiance received by tilted surfaces. These methods use horizontal irradiance components as inputs and apply transposition models to derive values on inclined planes. A key element in this process is the transposition factor, i.e., a dimensionless parameter that expresses the ratio between global irradiance on the tilted surface (G_T) and that on the horizontal plane (G_H). This factor depends on both the orientation of the receiving surface and the solar position.

The literature offers a wide range of transposition models, from basic isotropic formulations to more sophisticated anisotropic approaches. For instance, the isotropic model proposed by Liu and Jordan [9] assumes a uniform distribution of diffuse radiation across the sky dome. In contrast, anisotropic models, such as the Hay and Davies method [10] and its enhanced variant, the HDKR model [11], introduce directional dependencies by dividing the diffuse component into multiple parts. Specifically, the HDKR approach improves accuracy by partitioning the diffuse irradiance into separate contributions, thereby describing the non-uniform characteristics of sky brightness more effectively. Hence, diffuse irradiance is described as a combination of:

- an isotropic portion, uniformly received from the sky dome;
- a circumsolar component, which accounts for forward scattering near the solar disc;
- a horizon brightening term, representing enhanced irradiance near the skyline.

In this study, a more advanced and accurate methodology is adopted through the implementation of the Perez All-Weather Sky Model (AWM) [12]. The Perez model improves upon both isotropic and earlier anisotropic models by incorporating empirical data to account for circumsolar and horizon brightening effects under varying atmospheric conditions. Unlike Liu-Jordan or HDKR, it dynamically adjusts the sky luminance distribution based on sky clearness and brightness, enabling more precise irradiance transposition.

When estimating annual solar energy availability, a significant portion of the total insolation can arise from solar radiation reflected by surrounding surfaces. Since all materials reflect a fraction of the incident solar irradiance, this reflected energy may subsequently reach neighbouring elements, including solar energy systems. This component is typically characterised by the surface albedo (ρ), defined as the ratio of reflected to incident global radiation. While it is common in modelling to assume a spatially uniform and constant albedo for simplification, albedo is, in reality, dependent on both wavelength and angle of incidence. These spectral and angular variations can substantially affect the distribution and intensity

of reflected irradiance, which is particularly relevant for PV systems sensitive to rear-side exposure, such as bifacial modules [13].

3. METHODOLOGY

This chapter outlines the methodology adopted to compute annual solar insolation within the QGIS environment, using the Solar Energy on Building Envelopes (SEBE) model algorithms implemented through the Urban Multi-scale Environmental Predictor (UMEP) plugin. The following sections provide a detailed description of the input resources, the solar radiation modelling approach, and the formulation of profitability indices used for the comparative assessment of rooftop suitability (Figure 1).

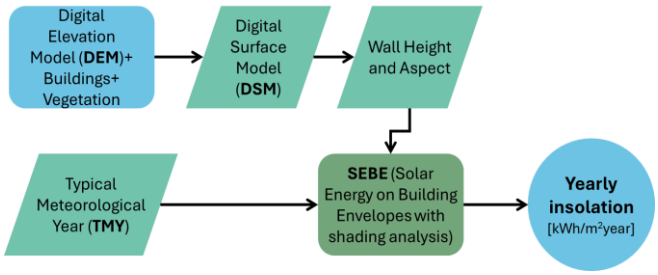

Figure 1. Schematic representation of the proposed methodology for assessing rooftop solar potential

3.1 Input resources

This chapter introduces the primary input resources employed in the present analysis, including raster datasets, vector layers, and Typical Meteorological Year (TMY) data, which together form the foundation for the spatial and climatic characterisation of the study area.

Raster data are structured as matrices composed of regularly sized pixels, each representing a specific spatial area. These data types are particularly well-suited for representing variables that change continuously across space, such as temperature, elevation, or land cover. The spatial resolution of a raster dataset is determined by the size of its individual pixels, with smaller pixel sizes providing finer spatial detail. In this study, the analysis is based on two types of raster files: the Digital Elevation Model (DEM) and the DSM. These raster datasets represent the Earth's surface in image form, where each pixel corresponds to a specific elevation value at a defined geographic location, referenced by latitude and longitude. A DEM provides a three-dimensional digital representation of the terrain surface, capturing detailed information on topographic features such as elevation and surface variation. They are generated by dividing the surface into a grid of cells or points, each assigned an elevation attribute. The accuracy and spatial resolution of DEMs depend on the quality and source of the input data. The DSM is a three-dimensional digital representation of the Earth's surface: unlike the DEM, the DSM includes all features present above the bare ground, such as buildings, vegetation, and both natural and artificial structures, thereby representing the topmost surface layer. In this analysis, DSM files are derived from recent LiDAR surveys and consist of 0.5 × 0.5 m² raster data.

The second type of data employed in this study consists of vector files. Unlike raster data, which are pixel-based, vector files represent real-world objects using geometric elements such as points, lines, and curves, defined by coordinates and mathematical instructions that allow for rendering shapes accurately. These files are widely used for applications requiring high resolution and scalability, as their mathematical basis allows for resizing without loss of quality. From the Geoportal of the Municipality of Genoa (https://mappe.comune.genova.it/MapStore2/#/), not only DEM and DSM raster layers are available, but also building footprints, as well as vectors representing several infrastructures. The building polygons include height attributes, which can be accessed through QGIS by selecting individual features and the attribute table (Figure 2).

Finally, TMY data were obtained from the PVGIS platform [14] and are based on the ERA5 database, chosen for compatibility with the UMEP plugin. The database encompasses data for the period 2005-2023 and results in an annual global horizontal insolation ($H_{tot,H,y}$) of approximately 1445 kWh/m^2; the diffuse component ($H_{diff,H,y}$) accounts for 490 kWh/m^2.

Figure 2. Vector layer of buildings overlaid on the orthophoto of the Albaro district (DSM 3930), Genoa, Italy

3.2 Insolation model description

The SEBE plugin enables the estimation of annual solar exposure on urban surfaces while considering the 3D morphology of the city. Initially, raster files representing the height and azimuthal orientation of each pixel are obtained, which are then used to generate slope rasters (Figure 3). This raster becomes one of the inputs for the Daily Shadow Pattern tool, which calculates the shadowing effects.

Figure 3. Slope raster used for shadow computation

Using the well-established method introduced by Ratti and Richens [15], the sun's path through the sky is simulated throughout the year at regular intervals and a shadow factor S for each pixel is defined according to Eq. (2). The shadow

factor is calculated based on binary shadow values from buildings (S_B) and vegetation (S_V), and by considering vegetation transmissivity (τ).

$$S = S_B - (1 - S_V) \cdot (1 - \tau) \quad (2)$$

The shadow factor assumes values between 0 (i.e., pixel completely shaded) and 1 (i.e., pixel not shaded). Thus, the visibility of the sun for each DSM cell is assessed for each time step, accounting for all the available obstructions. In this analysis, shadow calculations are performed at 30-minute intervals and the shadow map is created by generating a Boolean image.

For the calculation of solar irradiance, the meteorological data is pre-processed and redistributed into 145 patches of similar solid angles throughout the sky vault according to the well-known approach presented by Lindberg et al. [16]; this approach has been adopted for numerous analyses of solar potential and the effects of tilt and orientation, as the recent paper by Ferry et al. [17]. Through this cumulative sky approach, the sky dome is represented by aggregating solar radiation data over time for each patch, allowing for a detailed assessment of solar exposure on surfaces with varying orientations and inclinations (Figure 4).

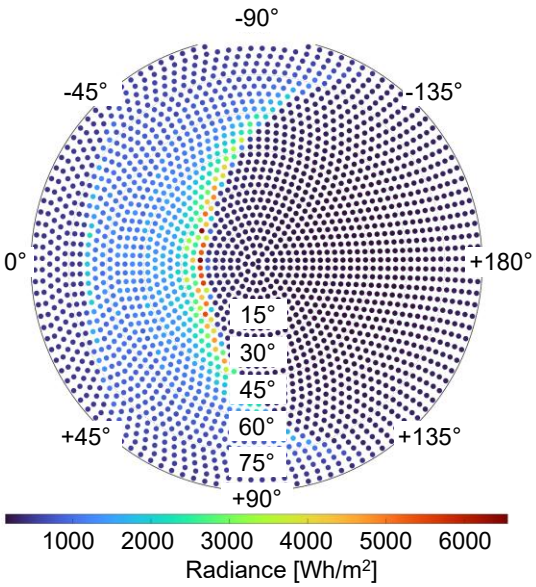

Figure 4. Cumulative sky model generated for the city of Genoa based on PVGIS–ERA5 data, processed using MATLAB

To redistribute the direct component of solar radiation, the position of the sun is computed for each time step using the meteorological dataset. The solar position is then projected onto the sky dome and assigned to the centroid of the nearest sky patch among the 145 discrete elements defined by the default SEBE sky subdivision scheme. The model assumes that the direct irradiance originates from the solar disk center as it traverses the sky vault. In parallel, the diffuse component is spatially distributed over the sky dome using the Perez AWM, which provides a relative luminance distribution *lv* for the i^{th} sky element depending on the position of the sun and the meteorological conditions at the given moment, as in Eq. (3).

$$lv_i = \left[1 + a \cdot \exp\left(\frac{b}{\cos\theta_i}\right)\right] \cdot [1 + c \cdot \exp(d \cdot \chi_i) + e \cdot \cos^2\chi_i] \quad (3)$$

Relative irradiance is defined based on the zenith angle of each sky element (θ_i), the angle between the sky element and the position of the sun (χ_i) and a set of coefficients dependent on the insolation conditions: a is related to the horizon brightening or darkening, b to the horizontal gradient of luminance, c to the circumsolar intensity, d to the circumsolar width and e to the backscattering light on earth surface.

Absolute irradiance values (Lv_i) for each of the N sky patches, defined by their respective solid angles Ω_i, are computed such that their cumulative contribution, when projected onto a horizontal surface, matches the total diffuse irradiance at ground level (G_{diff}), as expressed in Eq. (4). The model then incorporates the direct irradiance component by adding an additional element corresponding to the solar disk's position on the sky vault.

$$Lv_i = lv_i \cdot \frac{G_{diff}}{\sum_{i=1}^{N} lv_i \cdot \Omega_i \cdot \cos\theta_i} \quad (4)$$

Finally, the calculation of the global irradiance $G_{tot,T}$ is based on the summation of the beam, diffuse and reflected contributions associated with each sky element i, as expressed in Eq. (5).

$$G_{tot,T} = \sum_{i=1}^{N} [G_{b,H} \cdot \cos\theta_w \cdot S + G_{diff,H} \cdot S + G_{tot,H} \cdot (1 - S) \cdot \rho]_i \quad (5)$$

In detail:

- Subscripts *tot*, *b*, and *diff* refer to total, beam and diffuse irradiance;
- Subscripts T and H distinguish between tilted (T) and horizontal (H) surfaces;
- S is the previously introduced shadow factor;
- θ_w is the incidence angle, i.e. the zenith angle of the sun with respect to a tilted surface;
- ρ is the albedo of the surroundings, here assumed equal to 0.15.

3.3 Indicators for PV roof suitability

The output generated by the SEBE algorithm consists of a detailed dataset in which each rooftop is identified along with a set of attributes, including:

- Roof ID;
- Total roof area;
- Average insolation across the roof pixels;
- Minimum and maximum pixel insolation values per roof;
- Standard deviation of insolation among the pixels representing each roof;
- Median insolation value across the roof pixels.

To refine the analysis and filter non-relevant surfaces, specific thresholds were established. Only rooftops with an area exceeding 50 m² were considered, and minimum annual insolation thresholds ranging from 1000 to 1500 kWh/m² were applied, as further detailed in the results section.

Based on the insolation output data, this study proposes an overall index for rooftop solar utilisation potential (Φ_r), with the aim of supporting decision-makers, policymakers, private

citizens, and businesses in identifying the most promising surfaces for decentralized renewable energy production, particularly within the framework of RECs. This unified indicator, developed in reference to the case study of the Albaro district in Genoa, enables comparative assessments at broader urban or regional scales for evaluating solar potential across different parts of the city. Specifically, as detailed in the following equation, the indicator is derived from the normalized linear combination of three distinct variables, each rescaled using min-max normalization as shown in Eq. (6). In the following, an asterisk superscript will be used to denote variables that have been rescaled using min–max normalization.

$$x* = \frac{x - x_{\min}}{x_{\max} - x_{\min}} \tag{6}$$

The three variables used to compute the index Φ_r are described in detail as follows:

- The annual average insolation received by rooftop r ($\bar{H}_{y,r}$);
- The effective rooftop area of r receiving annual insolation values above a predefined threshold th [kWh/m²/yr] (A_r^{th});
- A solar uniformity index (U_r), expressed by Eq. (7) and derived from the ratio of the standard deviation to the mean insolation: in this case, the standard deviation is calculated based on the annual insolation values of each pixel p within the set of pixels P_r corresponding to rooftop r, with reference to the average insolation of the same roof.

$$U_r = 1 - \frac{\sqrt{\sum_{p=1}^{P_r} \left(H_{y,p} - \bar{H}_{y,r}\right)^2}}{\bar{H}_{y,r} \cdot \sqrt{P_r}} \tag{7}$$

Finally, the index for rooftop solar utilisation potential Φ_r is determined according to Eq. (8) by weighing the three variables mentioned using numerical constants w_1, w_2, and w_3, which in this study take the values provided in Table 1.

$$\Phi_r = w_1 \cdot \left(\bar{H}_{y,r}\right)^* + w_2 \cdot (A_r^{th})^* + w_3 \cdot (U_r)^* \tag{8}$$

Table 1. Weight coefficients for Φ_r calculation

	Value	Weight
w_1	0.3	Yearly average insolation
w_2	0.3	Roof area
w_3	0.4	Insolation uniformity

4. RESULTS

4.1 Assessment of the solar potential

A total of 3,565 rooftops were analysed in the study area. Of these, only 1,229 possess more than 50 m² of surface area receiving annual solar irradiation above the threshold of 1,000 kWh/m², corresponding to approximately 34% of the total rooftop dataset. When varying the insolation threshold, the number of rooftops meeting the minimum criteria changes accordingly, as summarised in Table 2. The preliminary results underscore the significant potential for rooftop PV energy generation within the neighbourhood under investigation, which covers just under 3 km² (Figure 5). Based solely on rooftops exceeding the 1,000 kWh/m² insolation threshold, the total usable surface is approximately equal to 286,000 m²: considering an yearly average peak power per unit area equal to 160 W_p/m² to take into account spacing between modules and not usable areas of the roofs, this corresponds to available space for 45 MW_p of PV plants. For reference, the entire province of Genoa had an installed PV capacity of approximately 53 MW_p as of the end of 2023, indicating that this single urban district could play a meaningful role in scaling up local solar energy production.

Table 2. Total number of roofs above selected thresholds of surface (> 50 m²) and insolation

Yearly Insolation Threshold [kWh/m²/yr]	Number of Roofs above Threshold	Share of Total Number of Roofs
No threshold	1776	49.8%
1000	1229	34.5%
1100	1229	34.5%
1200	1227	34.4%
1300	1218	34.2%
1400	1190	33.4%
1500	1082	30.4%

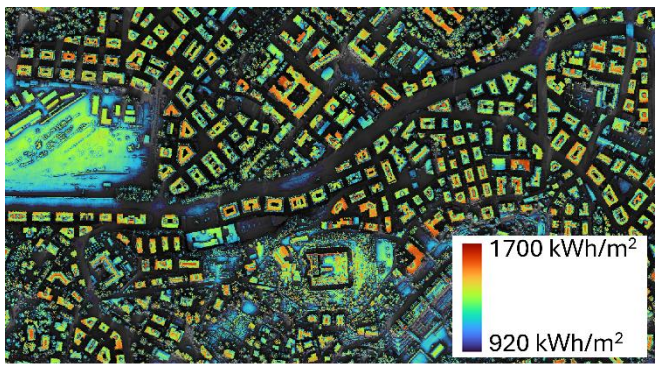

Figure 5. Insolation map resulting from yearly analysis of radiation data; a threshold at 920 kWh/m² has been applied

Despite the lack of wide flat surfaces, this urban district is characterised by a complex topography of hills and valleys, combined with a dense urban fabric. In urban solar potential analyses, a common issue is the possible influence of distant obstructions not included within the analysed DSM tile. In this study, particular attention was given to Monte Fasce, a mountain located northeast of the district, which could affect early morning irradiance. To assess this, a comparative simulation including both the DSM tile and the mountain was performed: results showed that the impact on annual insolation was negligible (always lower than 0.1%) due to the mountain's orientation relative to the southwest-facing study area [18].

As represented in the output insolation raster (Figure 5), train stations, industrial zones, and infrastructural areas often exhibit substantial solar potential. These areas typically lack the densely built-up configurations known as urban canyons, where tall, closely spaced buildings create persistent shading. As a minimum irradiance threshold is applied in the insolation map, darker areas represent lower annual insolation values and effectively highlight zones with limited solar potential, including shaded narrow streets and dense building clusters typical of urban canyon environments. Conversely, the

yellow-red zones, often corresponding to large rooftops and open areas, are better candidates for PV installations.

From a methodological perspective, it is important to note that this value requires further refinement through subsequent analyses aimed at accounting for potential obstructions (partially considered through penalties in the previously introduced uniformity index), as well as constrained surfaces and those already occupied by existing PV installations.

4.2 Statistical analysis of the results

The distributions shown in Figure 6 illustrate the behaviour of the probability density function as a function of the percentage of rooftop area receiving insolation above the threshold values indicated in the legend. By representing the probability (vertical axis) that a given percentage of a rooftop (horizontal axis) exceeds a specified insolation threshold, this analysis highlights how the selected threshold significantly affects the distribution itself. Specifically, approximately 7 out of 10 rooftops have more than 75% of their surface area with insolation exceeding 1,000 kWh/m², whereas only 2 rooftops have more than 50% of their area exposed to insolation greater than 1,500 kWh/m². In general, higher insolation thresholds cause the curve to shift leftward, indicating that fewer buildings meet the elevated requirements, thereby emphasising rooftops with extensive, well-irradiated surfaces.

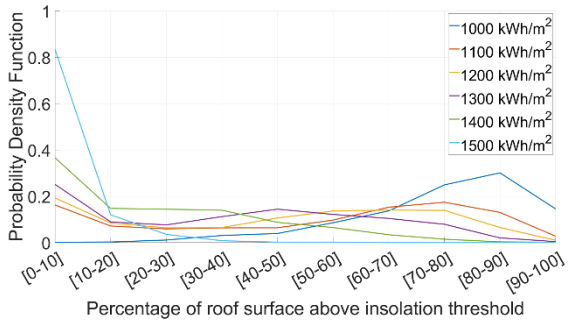

Figure 6. Probability density function representing the roofs' usable surface area at different insolation thresholds

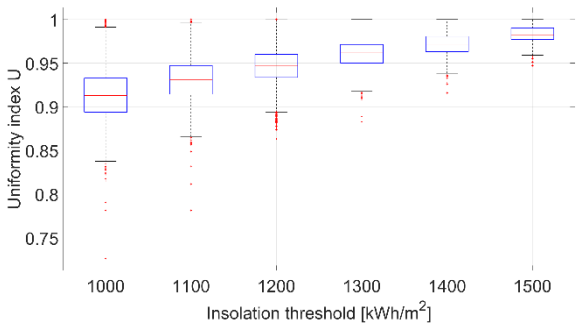

Figure 7. Boxplot representing the distribution of insolation uniformity index *U* at different insolation thresholds

The impact of the chosen irradiance thresholds is also evident when analysing the outputs in terms of the solar irradiance uniformity index *U* (Figure 7). The results reveal distinct patterns across rooftops and varying thresholds: as the minimum irradiance threshold increases, irradiance distribution becomes more uniform, primarily due to the exclusion of lower-performing rooftop areas from the analysis. Including solar energy uniformity in rooftop assessments is essential, as significant variations across a single surface can lead to efficiency losses in PV systems due to mismatch effects and suboptimal module performance.

4.3 Index for solar utilisation potential Φ_r

Finally, by combining multiple indicators as presented in Eq. (8), rooftops can be compared to identify those most suitable for PV installations, with the aim of maximising distributed generation and evaluating self-consumption potential within the framework of RECs. Based on the results, four rooftops were identified with an index for solar utilisation potential Φ_r greater than 0.6, standing out as those with the highest potential for solar applications across the study area. Additionally, the majority of rooftops (703 units, accounting for 57% of the total) fall within the 0.4–0.5 range, providing a useful characterisation of the average solar potential across the study area. The results of this investigation are summarised in Figure 8, where the horizontal axis represents the roof area above the insolation threshold, the vertical one the insolation uniformity index and the bubble dimension is proportional to the average insolation itself. In this analysis, the variables were weighted according to the coefficients shown in Table 1; however, the authors emphasise that this approach is suitable for future sensitivity analyses aimed at identifying the most appropriate weighting strategy. It also allows for comparative assessments across different districts within the city.

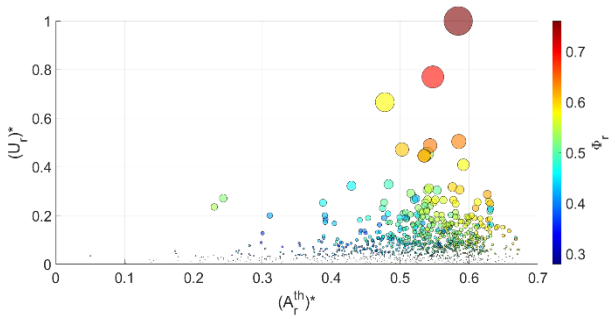

Figure 8. Bubble plot representing the index for solar utilisation potential Φ_r

5. CONCLUSIONS

The present study aims to provide a comprehensive understanding of the algorithms implemented in the UMEP plugin for QGIS, with the goal of evaluating the potential for PV installations at the urban scale. The analysis focuses on the Albaro district, a selected neighbourhood in the city of Genoa, Italy, with particular attention to the relevance of PV solutions within the framework of newly established RECs, where the spatial relationship between production and consumption significantly influences incentive allocation.

In the initial phase, filtering thresholds were applied, including minimum values for rooftop surface receiving sufficient solar exposure and a minimum annual solar irradiance per unit area, as derived from cumulative sky modeling based on TMY data. This pre-processing step enabled the identification of approximately 34% of the rooftops included in the study area's building vector layer as suitable candidates. The primary outcome was the generation of a high-resolution (0.5 × 0.5 m²) solar potential map of the

neighborhood, capable of capturing the impact of adjacent buildings, urban vegetation, and distant obstructions on annual insolation. Although beyond the main scope of this work, the map also allows the identification of urban canyons, i.e. areas where vertical PV installations would be particularly unfeasible due to persistent shading.

The overall solar potential of the filtered rooftops was found to be comparable to the total installed PV capacity across the entire province of Genoa (approximately 1,800 km²), underscoring the significance of urban PV deployment. A statistical analysis was subsequently conducted to examine the influence of the applied thresholds on the distribution of suitable roof surfaces and the uniformity of insolation, revealing clear patterns depending on the irradiance criteria.

Finally, a composite index of solar utilisation potential was computed for each rooftop, based on a linear combination of annual insolation, usable area, and irradiance uniformity. While 703 of the 1,229 qualified rooftops showed index values between 0.4 and 0.5, a smaller subset demonstrated high suitability for PV deployment, thus enabling a prioritisation of rooftops for future distributed solar energy projects.

ACKNOWLEDGMENT

This research is a part of the Italian National Program PNNR NEST Spoke 8 CUP D33C22001330002.

REFERENCES

[1] Masson, G., Van Rechem, A., de l'Epine, M., Jäger-Waldau, A. (2025). Snapshot of global PV markets 2025. International Energy Agency Photovoltaic Power Systems Programme. https://doi.org/10.69766/pbhv9141

[2] Fina, B., Auer, H., Friedl, W. (2020). Cost-optimal economic potential of shared rooftop PV in energy communities: evidence from Austria. Renewable Energy, 152: 217-228. https://doi.org/10.1016/j.renene.2020.01.031

[3] Doignon, Y., Blöss-Widmer, I., Ambrosetti, E., Oliveau, S. (2023). Spatial distribution of population and urbanisation. In Population Dynamics in the Mediterranean. SpringerBriefs in Population Studies. Springer, Cham. https://doi.org/10.1007/978-3-031-37759-4_2

[4] Freitas, S., Catita, C., Redweik, P., Brito, M.C. (2015). Modelling solar potential in the urban environment: state-of-the-art review. Renewable and Sustainable Energy Reviews, 41: 915-931. https://doi.org/10.1016/j.rser.2014.08.060

[5] Memme, S., Fossa, M. (2024). A novel approach for incidence angle modifier calculation of arbitrarily oriented linear Fresnel collectors: Theory, simulations and case studies. Renewable Energy, 222: 119857. https://doi.org/10.1016/j.renene.2023.119857

[6] Memme, S., Fossa, M., Rousse, D. (2025). Best tilt of PV system in Canada: Effect of the sky radiation model and climate conditions. Renewable Energy, 254: 123716. https://doi.org/10.1016/j.renene.2025.123716

[7] Desthieux, G., Carneiro, C., Camponovo, R., Ineichen, P., Morello, E., Boulmier, A., Abdennadher, N., Dervey, S., Ellert, C. (2018). Solar energy potential assessment on rooftops and facades in large built environments based on LiDAR data, image processing, and cloud computing. Methodological background, application, and validation in Geneva (solar cadaster). Frontiers in Built Environment, 4: 14. https://doi.org/10.3389/fbuil.2018.00014

[8] Giorio, M., Manni, M., Köker, N.I., Bertolin, C., Thebault, M., Lobaccaro, G. (2025). Interactive platforms for solar energy planning in smart cities: A state-of-the-art review of solar cadasters. Solar Energy, 287: 113227. https://doi.org/10.1016/j.solener.2024.113227

[9] Liu, B., Jordan, R. (1961). Daily insolation on surfaces tilted towards equator. ASHRAE J. (United States), 10: 53-59.

[10] Hay, J.E. (1993). Calculating solar radiation for inclined surfaces: Practical approaches. Renewable Energy, 3(4-5): 373-380. https://doi.org/10.1016/0960-1481(93)90104-O

[11] Reindl, D.T., Beckman, W.A., Duffie, J.A. (1990). Evaluation of hourly tilted surface radiation models. Solar Energy, 45(1): 9-17. https://doi.org/10.1016/0038-092X(90)90061-G

[12] Perez, R., Ineichen, P., Seals, R., Michalsky, J., Stewart, R. (1990). Modeling daylight availability and irradiance components from direct and global irradiance. Solar Energy, 44(5): 271-289. https://doi.org/10.1016/0038-092X(90)90055-H

[13] Parenti, M., Memme, S., Fossa, M. (2025). Sky radiance distribution based model for rear and front insolation estimation on PV bifacial modules. Solar Energy Materials and Solar Cells, 289: 113677. https://doi.org/10.1016/j.solmat.2025.113677

[14] Huld, T., Müller, R., Gambardella, A. (2012). A new solar radiation database for estimating PV performance in Europe and Africa. Solar Energy, 86(6): 1803-1815. https://doi.org/10.1016/J.SOLENER.2012.03.006

[15] Ratti, C., Richens, P. (1999). Urban texture analysis with image processing techniques. In Computers in Building: Proceedings of the Eighth International Conference on Computer Aided Architectural Design Futures. Boston, MA: Springer US, pp. 49-64. https://doi.org/10.1007/978-1-4615-5047-1_4

[16] Lindberg, C.F., Tan, S., Yan, J., Starfelt, F. (2015). Key performance indicators improve industrial performance. Energy Procedia, 75: 1785-1790. https://doi.org/10.1016/j.egypro.2015.07.474

[17] Ferry, A., Parenti, M., Thebault, M., Ménezo, C., Fossa, M. (2025). Optimal tilt angles for bifacial photovoltaic plants across Europe based on cumulative sky and typical meteorological year data. Solar Energy, 293: 113475. https://doi.org/10.1016/j.solener.2025.113475

[18] Memme, S., Lepore, D., Priarone, A., Fossa, M. (2024). Estimating the solar potential of the rooftops of the city of Genova through the 3D modelling of the built environment and anisotropic tiled sky analysis. Journal of Physics: Conference Series, 2893(1): 012121. https://doi.org/10.1088/1742-6596/2893/1/012121

NOMENCLATURE

Symbols

a, b, c, d, e	Constants for cumulative sky model [-]

A	Area [m^2]
G	Irradiance [W/m^2]
H	Insolation [kWh/m^2]
lv	Relative luminance of a sky element
Lv	Luminance of a sky element [W/m^2sr]
p	Index for pixel [-]
P	Total number of pixel [-]
R_b	Beam radiation tilt factor [-]
S	Shadow factor [-]
U	Insolation uniformity index [-]
w_1, w_2, w_3	Constants Φ_r calculation [-]

Greek symbols

β	Tilt angle [°]
θ_w	Angle of incidence [°]
θ	Solar zenith angle [°]
θ_i	Zenith angle of the i^{th} sky element
ρ	Albedo [-]
τ	Vegetation transmissivity [-]
Φ	Profitability index [-]
χ_i	Angle between i^{th} sky element and the direction of the sun [rad]
Ω_i	Solid angle of the i^{th} sky element [sr]

Acronyms

AWM	All Weather Model
DEM	Digital Elevation Model
DSM	Digital Surface Model
DTM	Digital Terrain Model
GIS	Geographic Information System
HDKR	Hay, Davies, Klucher, Reindl
LiDAR	Light Detection and Ranging
PV	Photovoltaic
RECs	Renewable Energy Communities
SEBE	Solar Energy on Building Envelopes
TMY	Typical Meteorological Year
UMEP	Urban Multi-scale Environmental Predictor

Subscripts

B	Building
b	Beam
d	Daily
$diff$	Diffuse
H	Horizontal
h	Hourly
n	Normal
o	Above hearth's atmosphere
T	Tilted surface
tot	Beam + Diffuse
V	Vegetation

Superscripts

$*$	Min-max normalized variable
th	Threshold